

HDAC Inhibitors Alleviate Uric Acid-Induced Vascular Endothelial Cell Injury by Way of the HDAC6/FGF21/PI3K/AKT Pathway

Kaihao Wang, PhD, Youhong Zhang, MD, Min Zhou, MD, Yipeng Du, PhD, Peixin Li, PhD, Chang Guan, PhD, and Zheng Huang, PhD

Abstract: Uric acid (UA) accumulation triggers endothelial dysfunction, oxidative stress, and inflammation. Histone deacetylase (HDAC) plays a vital role in regulating the pathological processes of various diseases. However, the influence of HDAC inhibitor on UA-induced vascular endothelial cell injury (VECI) remains undefined. Hence, this study aimed to investigate the effect of HDACs inhibition on UA-induced vascular endothelial cell dysfunction and its detailed mechanism. UA was used to induce human umbilical vein endothelial cell (HUVEC) injury. Meanwhile, potassium oxonate-induced and hypoxanthine-induced hyperuricemia mouse models were also constructed. A broad-spectrum HDAC inhibitor trichostatin A (TSA) or selective HDAC6 inhibitor TubastatinA (TubA) was given to HUVECs or mice to determine whether HDACs can affect UA-induced VECI. The results showed pretreatment of HUVECs with TSA or HDAC6 knockdown-attenuated UA-induced VECI and increased FGF21 expression and phosphorylation of AKT, eNOS, and FoxO3a. These effects could be reversed by FGF21 knockdown. In vivo, both TSA and TubA reduced inflammation and tissue injury while increased FGF21 expression and phosphorylation of AKT, eNOS, and FoxO3a in the aortic and renal tissues of hyperuricemia mice. Therefore, HDACs, especially HDAC6 inhibitor, alleviated UA-induced VECI through upregulating FGF21 expression and then activating the PI3K/AKT pathway.

This suggests that HDAC6 may serve as a novel therapeutic target for treating UA-induced endothelial dysfunction.

Key Words: histone deacetylase 6, uric acid, endothelial dysfunction, fibroblast growth factor 21

(*J Cardiovasc Pharmacol*TM 2023;81:150–164)

INTRODUCTION

Uric acid (UA) is the end product of purine metabolism that produces from the metabolism of adenosine triphosphate and nucleotides. Hyperuricemia has contributed as a risk factor for cardiovascular and renal diseases.^{1–3} One of the key hypotheses is that hyperuricemia induces endothelial dysfunction,^{4,5} and endothelial dysfunction is closely related to the physiopathologic mechanisms underlying the occurrence of cardiovascular and renal diseases.^{3,6–8} Therefore, preventing UA-induced vascular endothelial cell injury (VECI) is an effective strategy for treating UA-induced cardiovascular and kidney diseases.

Histone deacetylases (HDACs) are defined as the enzymes that remove acetyl groups from lysine residues of both histone and nonhistone proteins.⁹ To date, 18 mammalian HDACs have been identified and are characterized into 4 classes. In general, HDACs act as an epigenetic regulator to deacetylate nucleosome histones and suppress gene expression. HDAC inhibitors enhance the level of histone acetylation and stimulate some gene expression. HDAC inhibitors have been considered as a new class of anticancer drugs. However, its application in cardiovascular has attracted more and more attention.¹⁰ A growing number of preclinical studies have shown the anti-inflammatory and cardioprotective effects of numerous HDAC inhibitors.^{11,12} It has been reported that HDAC inhibitors can reduce ischemia-reperfusion injury,¹³ myocardial hypertrophy,¹⁴ and cardiac fibrosis.¹⁵ However, most of these studies focus on the effects of class I HDACs (HDACs 1,2,3) inhibitors. For example, HDAC1 has been found to play a role in ischemia-reperfusion injury¹⁶ and myocardial fibrosis,¹⁵ while HDAC2 is considered to play an important role in myocardial hypertrophy¹⁴ and cardiac arrhythmia.¹⁷ HDAC3 is also involved in the development of heart failure,¹⁸ ventricular remodeling,¹⁹ and hypertension.^{14,20} However, as a class II HDACs, there are relatively few reports on the direct effects of HDAC6 on the heart, while some studies have shown the protective effect of HDAC6 inhibitors on vascular endothelium.^{21–24} Thorsten et al reported that inhibition of HDAC6 activity improved endothelial

Received for publication April 17, 2022; accepted September 9, 2022.

From the Department of Cardiology, The First Affiliated Hospital of Guangzhou Medical University, Guangzhou, China.

This work is supported by Guangzhou Health Science and technology project (2021A010175, 20171A010301) and Guangzhou Science and Technology Project (202102010177).

The authors report no conflicts of interest.

Supplemental digital content is available for this article. Direct URL citations appear in the printed text and are provided in the HTML and PDF versions of this article on the journal's Web site (www.jcvp.org).

Study design, experimental method development, and study execution were performed by Z. Huang and K. Wang. Material preparation and data collection were conducted by M. Zhou, Y. Zhang, and Y. Du. Data analysis and the first draft of the manuscript was prepared by P. Li and C. Guan. All authors edited and approved the final version of the manuscript.

Correspondence: Zheng Huang, PhD, Department of Cardiology, The First Affiliated Hospital of Guangzhou Medical University, Guangzhou, China (e-mail: huangzhengGY@126.com).

Copyright © 2022 The Author(s). Published by Wolters Kluwer Health, Inc. This is an open access article distributed under the terms of the Creative Commons Attribution-Non Commercial-No Derivatives License 4.0 (CCBY-NC-ND), where it is permissible to download and share the work provided it is properly cited. The work cannot be changed in any way or used commercially without permission from the journal.

function and prevented or reversed the development of atherosclerosis.²² Shigeki et al also reported that the inhibition of HDAC6 activity attenuated endothelial barrier dysfunction induced by thrombin.²¹ In addition, several studies have shown that HDAC6 inhibitors have anti-inflammatory and renal protective effects.^{25,26} Recent research highlighted that HDAC6 inhibition attenuated inflammatory response and oxidative stress²⁷ and prevented TNF- α -induced inflammatory injury in lung endothelial cells.²⁴ Inhibition of HDAC6 could suppress renal fibrosis,²⁸ alleviate acute kidney injury.²⁹ Therefore, HDAC6 is a potential target for endothelial diseases, and HDAC6 inhibitors may be a potential anti-inflammatory and antioxidative drugs in VECI.

However, it remains unknown whether HDAC inhibitors can alleviate UA-induced VECI and related organ damage. We presume that HDAC inhibitors, especially HDAC6 inhibitor, may serve as a novel agent for UA-induced VECI. Trichostatin A (TSA), a broad-spectrum HDAC inhibitor, has been reported to exert various cardiovascular protective effects, including inhibiting myocardial hypertrophy³⁰ and attenuating myocardial fibrosis.³¹ In addition, TSA exhibits multiple modalities of benefit for vascular endothelial cells.^{32,33} Therefore, in this study, by culturing UA-stimulated human umbilical vein endothelial cells (HUVECs) and constructing hyperuricemia mouse model, while given TSA treatment, we aimed to investigate whether HDAC6 inhibitor could alleviate UA-induced inflammation and VECI and elucidate the underlying mechanisms. The findings enhanced our understanding of UA-induced VECI and revealed a novel target for the treatment of hyperuricemia.

MATERIALS AND METHODS

Cell Culture and Treatment

HUVECs were supplied by the American Type Culture Collection (Manassas, VA, USA). The cells were cultured in endothelial cell growth medium (ECM) containing 10% fetal bovine serum (FBS; Gibco, BV000) and 1% penicillin/streptomycin (Invitrogen, CA, USA) and then maintained at 37°C and 5% CO₂. The medium was refreshed every 2–3 days. Before experimental treatments, HUVECs were cultured without fetal bovine serum for 24 hours.

UA crystallites (Sigma–Aldrich, St. Louis, MO, USA) were dissolved in 1 N NaOH solution. HUVECs were stimulated with multiple doses of UA (6, 9, 12 mg/dL) for 24 hours. TSA, selective HDAC1-3 inhibitor Mocetinostat (MGCD0103), and LY294002 (specific PI3K/AKT signaling pathway inhibitor) were obtained from Selleck Chemicals (Houston, TX, USA). HUVECs were pretreated with low dose (50 nM) or high dose (100 nM) of TSA, Mocetinostat (2 μ M), or LY294002 (50 μ M) in ECM for 2 hours before UA (12 mg/dL) stimulation. The control (CON) group consists of untreated HUVECs.

Cell Transfection

The small interfering RNA (siRNA)-FGF21 (si-FGF21-1, 5'-GCGGTACCTCTACACAGAT-3'; si-FGF21-2, 5'-CCTTGAAGCCGGGAGTTAT-3') and siRNA-HDAC6 (si-HDAC6-1, 5'-CGGAGGGUCCUUAUCGUAGAUTT-3'; si-

HDAC6-2, 5'-CCUCACUGAUCAGGCCAUUUTT-3'), constructed by Guangzhou RiboBio Co, Ltd, were transfected into HUVECs by Lipofectamine 2000 reagent (Invitrogen) according to the kit's protocol. After transfection for 48 hours, HUVECs were subjected to further analyses. Real-time quantitative PCR (RT-qPCR) was conducted to verify transfection efficiency.

Animal Treatments

Specific pathogen-free (SPF) male Kunming mice (weighing 20.0 \pm 2.0 g) were obtained from Guangdong Laboratory Animals Monitoring Institute (Guangzhou, China) and maintained according to the Institutional Animal Care and Use Committee (IACUC) of Guangzhou Medical College's guidelines. The study protocol was approved by the IACUC. After adaptive feeding for 1 week, the mice were randomly assigned to 4 groups (n = 15): CON group, Model group, TSA group, and selective HDAC6 inhibitor Tubastatin A (TubA) group. The Model, TSA, and TubA groups were subcutaneously injected with potassium oxonate (300 mg/kg) and intraperitoneally injected with hypoxanthine (200 mg/kg) every day at 9:00 AM.³⁴ The CON group was given the same amount of 0.5% CMC-Na solution. In the Model, TSA, and TubA groups, mice were, respectively, administered with vehicle, TSA (0.6 mg/kg/d),³⁵ or TubA (50 mg/kg/d)³⁶ intraperitoneally. The CON group was given the same amount of physiological saline. All experiments were repeated continuously for 14 days.

After 2 weeks of treatment, the mice were sacrificed. Then, the aorta, kidney, and liver were collected. Two-thirds of tissues were used for RNA and protein analyses, while the remaining tissues were fixed in 10% neutral-buffered formalin for histopathological evaluation.

Measurement of Blood Pressure

During the day of end of every week, the blood pressure of mice was recorded using the noninvasive tail-cuff method (COPA; Kent Scientific, Torrington, USA).³⁷ Mice were placed into chambers on a warm platform at least 30 minutes to ensure adaptation to the following procedure. Blood pressure was measured in a proper environment for 3 times, and the average value was taken.

Vascular Reactivity

Thoracic aortas of mice were isolated and cut into segments 2 mm in length. The aortic rings were mounted on a wire myograph (Model 620M; DMT, Copenhagen, Denmark) in 5 mL of Krebs buffer (Kanglang Biotechnology, Shanghai, China) at 37°C with 5% CO₂ in O₂. Changes in force generation were documented using a PowerLab data acquisition system (ADInstruments, Colorado Springs, CO). During experiments, integrity of aortas was assessed by stimulation with 60 mM of KCl. After the tension is stabilized at 2.0 mN, we add phenylephrine (Sigma–Aldrich, St. Louis, MO, USA) to the solution to precontract the vessel and the final concentration of phenylephrine was 3 μ mol/L. Once the vessels reached a stable maximum tension, acetylcholine (Ach; Sigma–Aldrich) with concentration gradient (1 nM–10 μ M) was added in turn. When the vasodilation of previous Ach concentration reached a

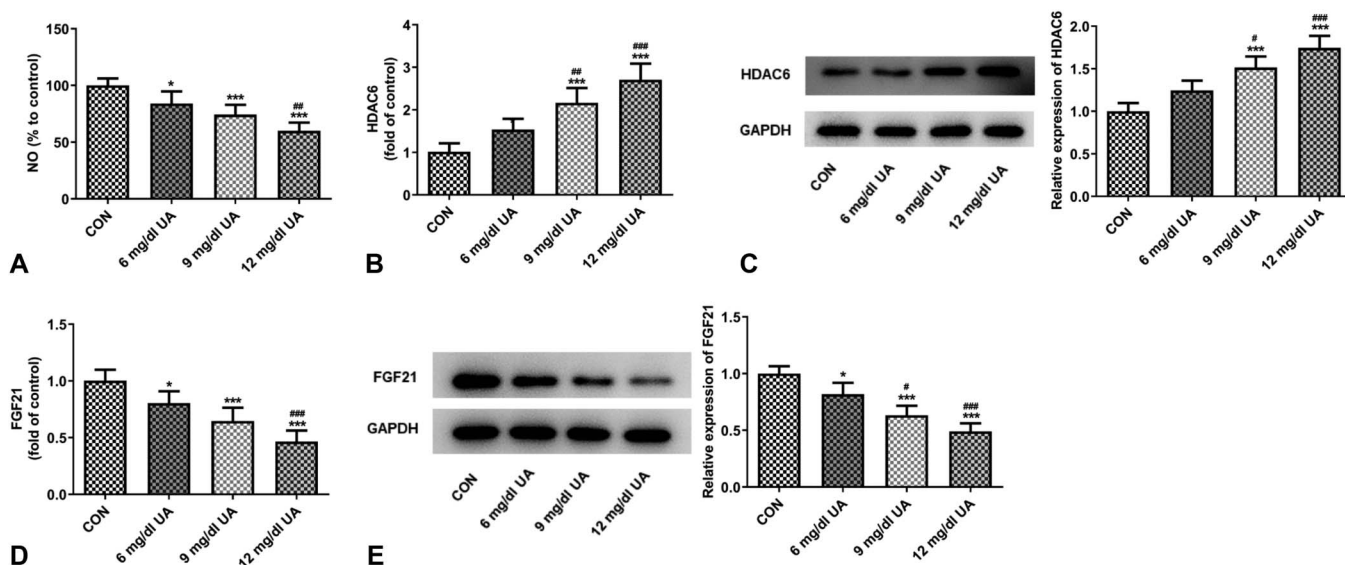


FIGURE 1. High UA levels stimulated HDAC6 and inhibited FGF21 expression in HUVECs. A, NO production detected by NO assay kit ($n = 5$). B, HDAC6 mRNA expression determined by RT-qPCR ($n = 5$). C, HDAC6 protein expression determined by WB analysis ($n = 4$). D, FGF21 mRNA level measured by RT-qPCR ($n = 5$). E, FGF21 protein level measured by WB analysis ($n = 4$). One-way ANOVA followed by Tukey's post hoc multiple-group comparisons. * $P < 0.05$, ** $P < 0.01$, *** $P < 0.001$ versus CON; # $P < 0.05$, ## $P < 0.01$, ### $P < 0.001$ versus 6 mg/dL UA.

relatively stable tension, we immediately added Ach solution of next concentration. Then, we released the Krebs solution and rinsed the vessels with Krebs solution for 3 times. During the last rinse, we slowly adjusted the tension to about 2.0 mN and then added phenylephrine to the final concentration of 3 $\mu\text{mol/L}$. When the vessels reached a stable maximum tension, sodium nitroprusside (SNP) from Sigma–Aldrich with concentration gradient (1 nM–10 μM) was added in turn. Once vasodilation of previous SNP concentration reached a relatively stable tension, we immediately added SNP solution of next concentration. GraphPad prism 8.0 software was used to plot the concentration effect curve and fitted the curve with S-type equation.

Histopathology

The formalin-fixed tissues were dehydrated in a graded alcohol series, cleared in xylene, embedded with paraffin, and sectioned into 5- μm thickness. The aortic and liver sections were subjected to hematoxylin and eosin (H&E) staining. Meanwhile, the kidney sections were performed by H&E, periodic acid–Schiff (PAS), and Masson's trichrome staining. The media thickness of thoracic aortas was assessed by measuring the length of the media at 10 different positions per animal at 200 \times magnification. Masson's trichrome staining was used to measure renal fibrotic content. Aortic media thickness and renal fibrotic area were quantified using ImageJ software.

RT-qPCR

Total RNA was extracted from HUVECs or mouse tissues by TRIzol method (Invitrogen). cDNA synthesis was conducted using the PrimeScript RT reagent kit (TaKaRa, Tokyo, Japan). The RT-qPCR conditions were 30 seconds at 95 $^{\circ}\text{C}$, followed by 40 cycles of 5 seconds at 95 $^{\circ}\text{C}$ and 30

seconds at 60 $^{\circ}\text{C}$. Levels of mRNA expression, including HDAC6, TNF- α , IL-1 β , IL-6, CD31, α -SMA, and FGF21, detected by a SYBR green qPCR assay kit (TaKaRa, Japan) were calculated by $2^{-\Delta\Delta\text{CT}}$ method after normalization to GAPDH. The primer pairs are listed in Supplementary Table 1, <http://links.lww.com/JCVP/A884>.

Western Blot (WB) Analysis

Total protein content was determined by BCA assay (Beyotime, Beijing, China). Then, the protein specimens were separated through 10% SDS-PAGE and transferred onto a PVDF membrane. After blocking with skimmed milk, the membrane was incubated with appropriate antibodies overnight at 4 $^{\circ}\text{C}$. The following primary antibodies were obtained from Abcam: HDAC1 (1:1000; ab109411), HDAC2 (1:1000; ab32117), HDAC3 (1:1000; ab32369), HDAC6 (1:1000; ab1440), AKT (1:1000; ab8805), p-AKT (1:500; ab38449), eNOS (1:1000; ab199956), p-eNOS (1:500; ab215717), FoxO3a (1:1000; ab70315), p-FoxO3a (1:500; ab47285), CD31 (1:1000; ab281583), α -SMA (1:1000; ab5694), and FGF21 (1:1000; ab171941). The primary antibody GAPDH (1:3000; 10494-1-AP) was purchased from Proteintech Group (Chicago, USA). After incubation with the primary antibodies, the membrane was rinsed 3 times and incubated with horseradish peroxidase–conjugated secondary antibody goat anti-rabbit immunoglobulin (1:5000; Zhongshanjinjiao, China). Finally, the membranes were visualized using an enhanced chemiluminescence kit (Beyotime Institute of Biotechnology), and their intensities were determined with ImageJ software.

HDAC Activity Assays

HDAC1 (Cat. No: GMS50082.2), HDAC2 (Cat. No: GMS50082.3), HDAC3 (Cat. No: GMS50082.4), and

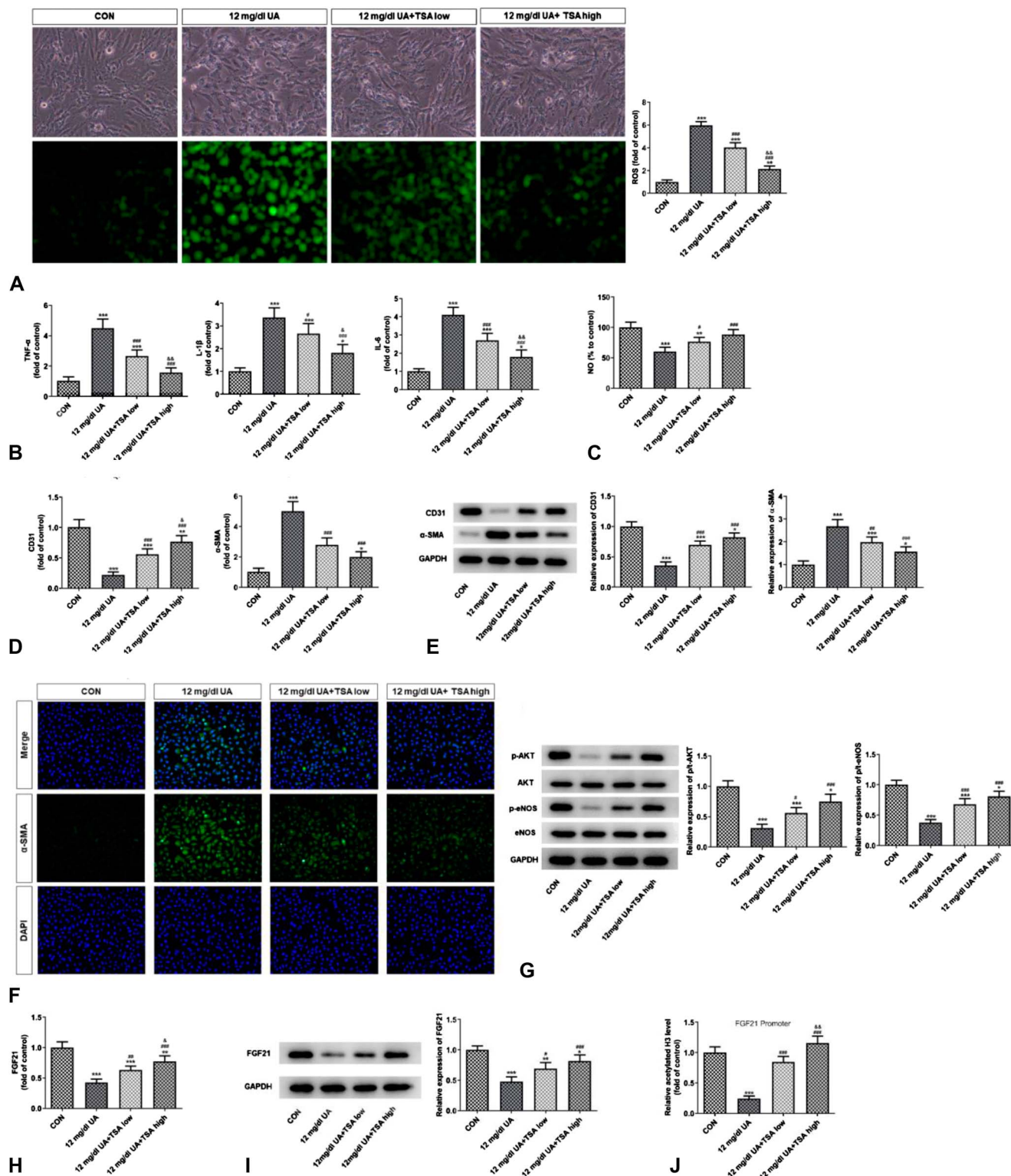


FIGURE 2. TSA attenuated UA-stimulated endothelial dysfunction in HUVECs. A, Representative cell morphology and ROS generation captured by a microscope (n = 3). B, TNF- α , IL-1 β , and IL-6 mRNA levels determined by RT-qPCR (n = 5). C, NO production (n = 5). D, RT-qPCR analysis of CD31 and α -SMA (n = 5). E, WB analysis of CD31 and α -SMA (n = 4). F, α -SMA expression analyzed by immunofluorescence (n = 3). G, WB analysis of p-AKT/AKT and p-eNOS/eNOS (n = 4). H, RT-qPCR analysis of FGF21 (n = 5). I, WB analysis of FGF21 (n = 4). J, Level of histone H3 acetylation on the FGF21 promoter region, as analyzed by ChIP (n = 4). One-way ANOVA followed by Tukey's post hoc multiple-group comparisons. * $P < 0.05$, ** $P < 0.01$, *** $P < 0.001$ versus CON; # $P < 0.05$, ## $P < 0.01$, ### $P < 0.001$ versus 12 mg/dL UA; &# $P < 0.05$, &## $P < 0.01$ versus 12 mg/dL UA+TSA low.

HDAC6 (Cat. No: GMS50082.7) activity were measured by HDAC1,2,3,6 colorimetric activity assay kit (GENMED SCIENTIFICS INC., USA) according to the kit's protocols. In brief, the nuclear extract of HUVECs was incubated with Color de Lys substrate at 37°C for 1 hour. The absorbance value was examined using a microplate reader at 405 nm.

HDAC1,2,3,6 activities were calculated based on the formula provided in the kit's protocols.

Serum Biochemical Analysis

The levels of NO (A012-1-2), UA (C012-1-1), creatinine (C011-2-1), and blood urea nitrogen (C013-2-1) in the

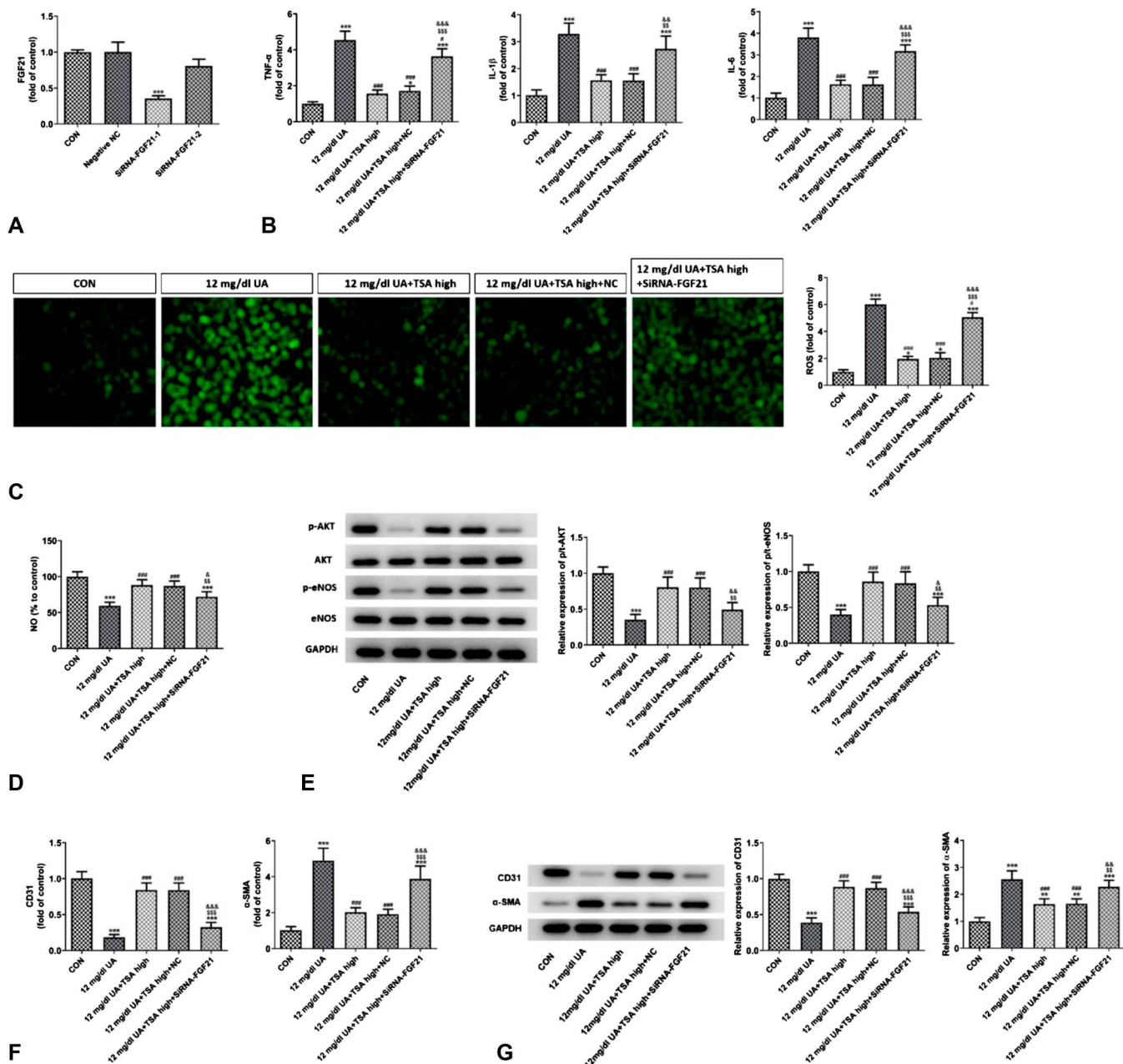


FIGURE 3. FGF21 knockdown abrogated the effects of TSA on UA-induced inflammation, oxidative stress, endothelial dysfunction, and endothelial-interstitial transformation in HUVECs. A, RT-qPCR analysis of FGF21 (n = 3). B, RT-qPCR analysis of TNF- α , IL-1 β , and IL-6 (n = 4). C, ROS generation (n = 3). D, NO production (n = 5). E, Levels of p-AKT/AKT and p-eNOS/eNOS measured by WB (n = 4). F, RT-qPCR analysis of CD31 and α -SMA (n = 4). G, WB analysis of CD31 and α -SMA (n = 4). One-way ANOVA followed by Tukey's post hoc multiple-group comparisons. * $P < 0.05$, ** $P < 0.01$, *** $P < 0.001$ versus CON; ### $P < 0.001$ versus 12 mg/dL UA; \$\$\$ $P < 0.01$, \$\$\$ $P < 0.001$ versus 12 mg/dL UA+TSA high; &# $P < 0.05$, &# $P < 0.01$, &#&# $P < 0.001$ versus 12 mg/dL UA+TSA high+NC.

serum were detected by special detection kits (Jiancheng Bioengineering Institute, China) according to the kit's protocols. The serum levels of FGF21 (CSB-EL008627MO), TNF- α (CSB-E04741m), and IL-6 (CSB-E04639m) were determined using the enzyme-linked immunosorbent assay (ELISA) kits (CUSABIO life Sciences, Wuhan, China) according to the kit's protocols.

Measurement of ROS Production

The intracellular level of reactive oxygen species (ROS) was assessed using a ROS assay kit (Jiancheng Bioengineering

Institute, China; E004-1-1). In brief, HUVECs coincubated with 25 mM L-Glu and 100 μ M 6-OHDA and then maintained with 10 μ M dichlorofluorescein diacetate (DCFH-DA, Sigma, MO, USA) at 37°C for 0.5 hours in the dark. DCFH-DA is oxidized to produce fluorescence in the presence of ROS. The fluorescent color was determined using a fluorescence microscope with excitation and emission wavelengths at 485 and 520 nm, respectively.

Immunofluorescence

HUVECs were fixed with 4% paraformaldehyde for 15 minutes. Subsequently, the cell membranes were

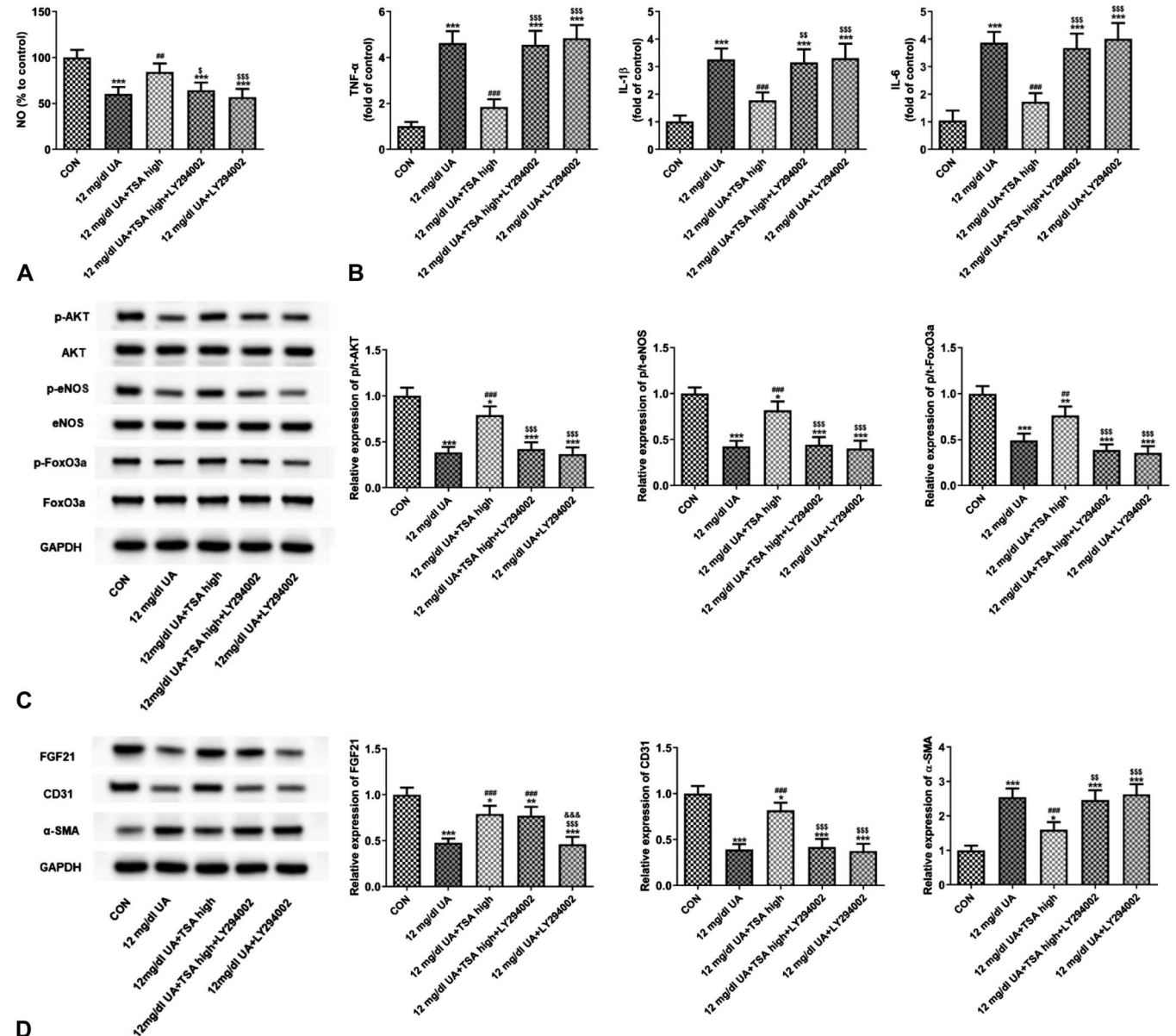


FIGURE 4. LY294002 abrogated the effects of TSA on UA-induced vascular endothelial cell injury in HUVECs. A, NO production (n = 5). B, Levels of TNF- α , IL-1 β , and IL-6 detected by RT-qPCR (n = 5). C, WB analysis of p-AKT/AKT, p-eNOS/eNOS, and p-FoxO3a/FoxO3a (n = 4). D, WB analysis of FGF21, CD31, and α -SMA (n = 4). One-way ANOVA followed by Tukey's post hoc multiple-group comparisons. * $P < 0.05$, ** $P < 0.01$, *** $P < 0.001$ versus CON; # $P < 0.01$, ### $P < 0.001$ versus 12 mg/dL UA; \$ $P < 0.05$, \$\$\$ $P < 0.01$, SSS $P < 0.001$ versus 12 mg/dL UA+TSA high; &#x&#xP < 0.001 versus 12 mg/dL UA+TSA high+ LY294002.

permeabilized using 0.2% Triton-x 100 for 15 minutes, and anti- α -SMA antibody (1:200; ab5694) was added at a dilution of 1:200 for overnight incubation at 4°C. After rinsing with PBS, the cells were incubated with Goat Anti-Rabbit IgG H&L (Alexa Fluor 594) secondary antibody (1:200; ab150080) at room temperature for 1 hour. DAPI (Sigma-Aldrich; Merck KGaA, Darmstadt, Germany) was used to stain nuclei for 5 minutes.

Chromatin Immunoprecipitation (ChIP) Assay

Chromatin Immunoprecipitation Assay (Saicheng Bioengineering Institute, Guangdong, China) was used to conduct the ChIP assay by following the kit's protocol. In brief, HUVECs were cross-linked with 1% formaldehyde for 30 minutes and stopped by 1.25 M glycine solution. HUVECs were harvested and ultrasonicated to generate 400–800 bp DNA fragment (Bioruptor Pico, Diagenode). Then, 10% of the broken

chromatin samples were placed into a new centrifuge tube as the input sample. The remaining part was added with 100 μ L ChIP buffer, reacted with acetylated histone H3 antibody (1:100, CST, #8173) or IgG (1:100, Santa Cruz, sc2025), and then mixed with the prepared magnetic beads for an incubation at 4°C overnight. The IP and input samples were mixed with 2 mL proteinase K at 60°C for 1 hour. After precipitating and purifying ChIP-enriched DNA fragments, quantitative PCR was conducted with FGF21 forward 5'-GCCAACCTGTCTCCCTCTG-3' and reverse 5'-GCTCAGATGCTCAGACCCTG-3'. The values were computed relative to a calibrator ($2^{-\Delta\Delta C_t}$) and normalized to the input sample.

Statistical Analysis

All data were presented as mean \pm SD and evaluated using the GraphPad Prism 8 software. Differences among

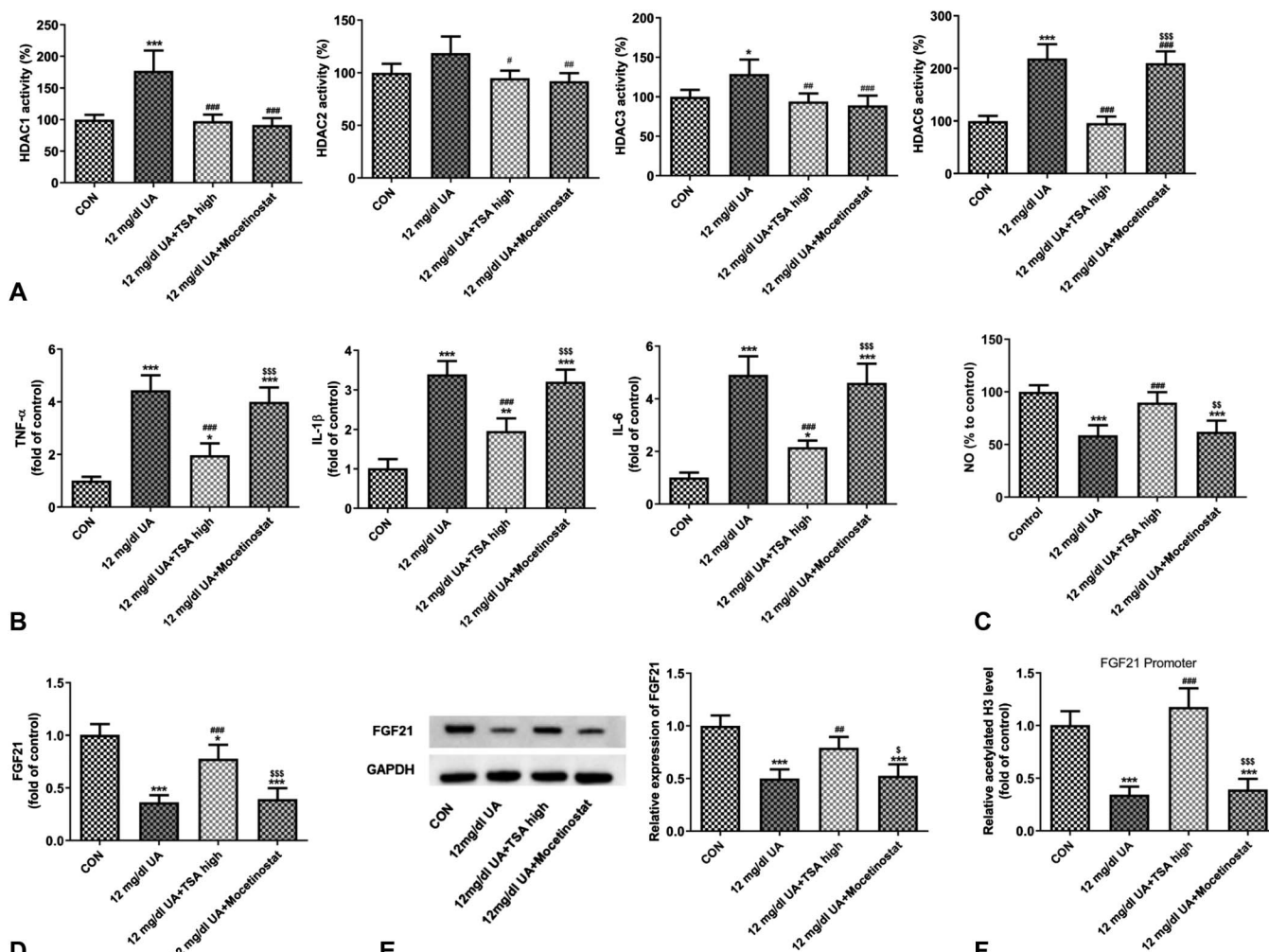


FIGURE 5. Different from TSA, Mocetinostat, a class-I selective HDAC inhibitor did not attenuate UA-stimulated endothelial dysfunction in HUVECs. A, HDAC1,2,3,6 activity detected by HDAC kits (n = 5). B, TNF- α , IL-1 β , and IL-6 mRNA level detected by RT-qPCR (n = 5). C, NO production (n = 5). D, RT-qPCR analysis of FGF21 (n = 5). E, WB analysis of FGF21 (n = 4). F, Level of histone H3 acetylation on the FGF21 promoter region, as analyzed by ChIP (n = 4). One-way ANOVA followed by Tukey's post hoc multiple-group comparisons. *P < 0.05, **P < 0.01, ***P < 0.001 versus CON; #P < 0.05, ##P < 0.01, ###P < 0.001 versus 12 mg/dL UA; \$P < 0.05, \$\$P < 0.01, \$\$\$P < 0.001 versus 12 mg/dL UA+TSA high.

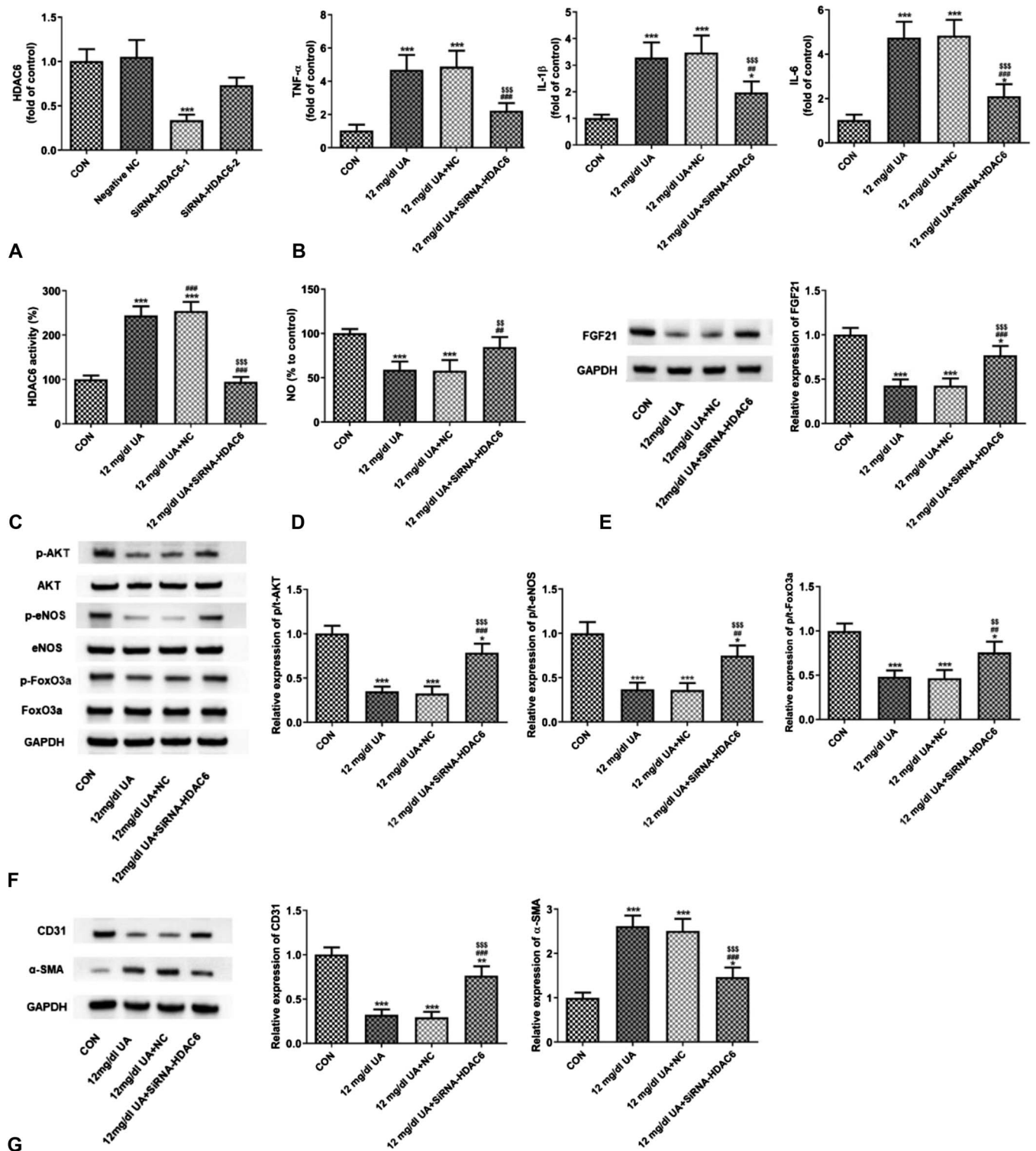


FIGURE 6. HDAC6 knockdown alleviated UA-induced inflammation, oxidative stress, endothelial dysfunction, and endothelial-interstitial transformation in HUVECs. A, HDAC6 mRNA level measured by RT-qPCR (n = 3). B, Levels of TNF- α , IL-1 β , and IL-6 detected by RT-qPCR (n = 5). C, HDAC6 activity (n = 5). D, NO production (n = 5). E, WB analysis of FGF21 (n = 4). F, WB analysis of p-AKT/AKT, p-eNOS/eNOS, and p-FoxO3a/FoxO3a (n = 4). G, WB analysis of CD31 and α -SMA (n = 4). One-way ANOVA followed by Tukey's post hoc multiple-group comparisons. * $P < 0.05$, ** $P < 0.01$, *** $P < 0.001$ versus CON; ## $P < 0.01$, ### $P < 0.001$ versus 12 mg/dL UA; \$\$\$ $P < 0.01$, \$\$\$\$ $P < 0.001$ versus 12 mg/dL UA+NC.

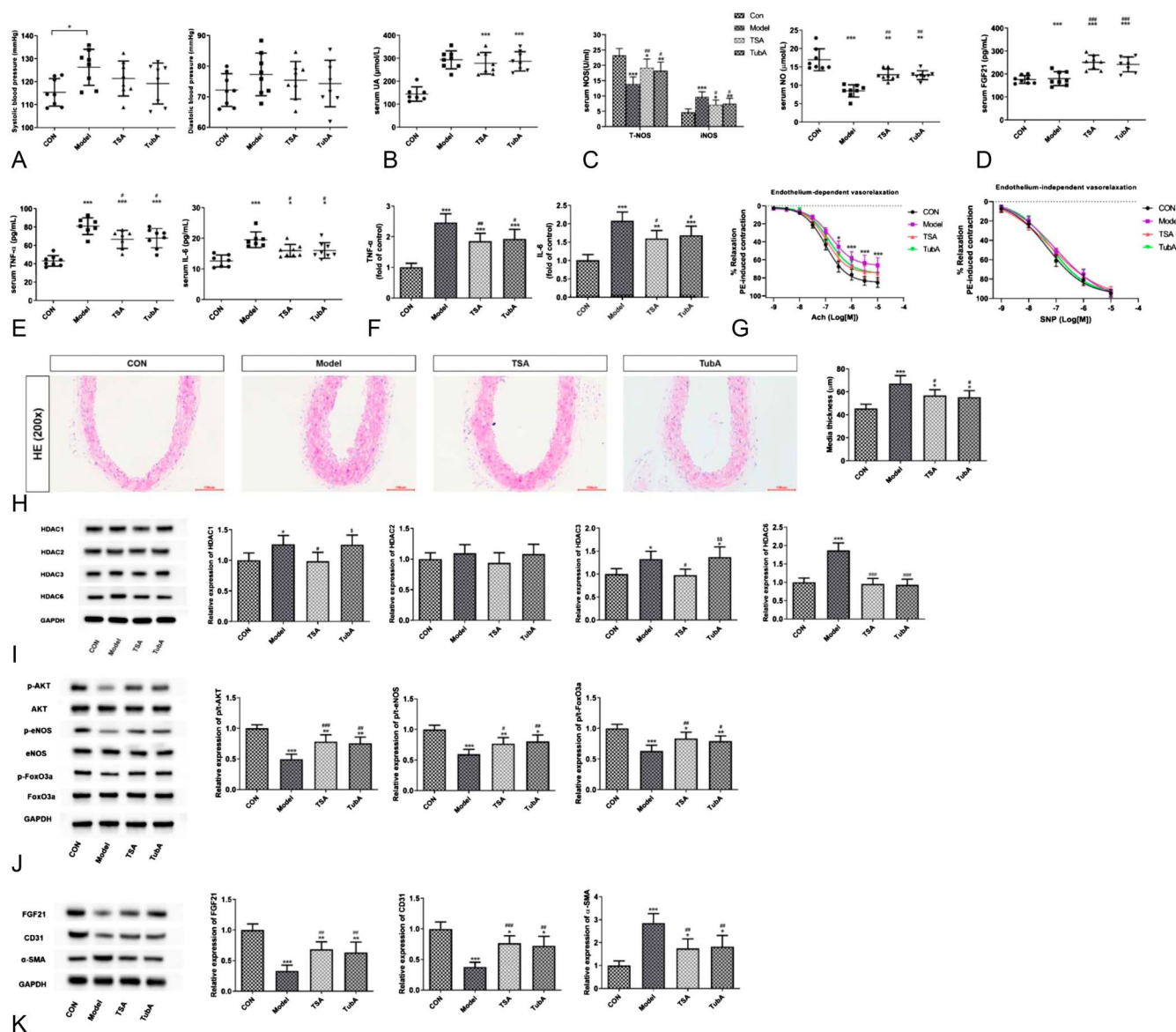


FIGURE 7. TSA or TubA alleviated aortic inflammation and dysfunction in hyperuricemic mice. A, Blood pressure between the groups (n = 15). B, Serum UA (n = 7–8). C, Serum NO (n = 8). D, Serum FGF21 (n = 7–8). E, Serum TNF- α and IL-6 (n = 7–8). F, Levels of TNF- α and IL-6 mRNA in aorta tissue were determined by RT-qPCR (n = 5). G, Vasorelaxant responses to Ach and SNP in mice aortic rings precontracted with phenylephrine (n = 5). H, Representative images of mice aorta histopathology through H&E staining (magnification $\times 200$) and used for analysis of media thickness. I, WB analysis of HDAC1, 2, 3, and 6 in aorta tissue (n = 5). J, WB analysis of p-AKT/AKT, p-eNOS/eNOS, and p-FoxO3a/FoxO3a in aorta tissue (n = 5). K, WB analysis of FGF21, CD31, and α -SMA in aorta tissue (n = 5). One-way ANOVA followed by Tukey’s post hoc multiple-group comparisons. * $P < 0.05$, ** $P < 0.01$, *** $P < 0.001$ versus CON; # $P < 0.05$, ## $P < 0.01$, ### $P < 0.001$ versus model; \$ $P < 0.05$, \$\$ $P < 0.01$ versus TSA.

groups were compared using the one-way ANOVA followed by a post hoc test. $P < 0.05$ was deemed statistically significant.

RESULTS

High UA Promotes HDAC6 and Inhibits FGF21 Expression in HUVECs

As presented in Figure 1A, UA stimulation reduced NO level in a concentration-dependent fashion compared with the

CON group (0 mg/dL UA). As shown in Figure 1B, C, UA stimulation significantly increased HDAC6 expression in a concentration-dependent fashion compared with the CON group. In addition, the protein and mRNA levels of FGF21 were remarkably downregulated after UA stimulation (Fig. 1D, E).

HDAC Inhibitor TSA Attenuates UA-stimulated Endothelial Injury in HUVECs

To test whether HDACs are involved in hyperuricemia pathophysiology, the HDAC inhibitor, TSA, was used in

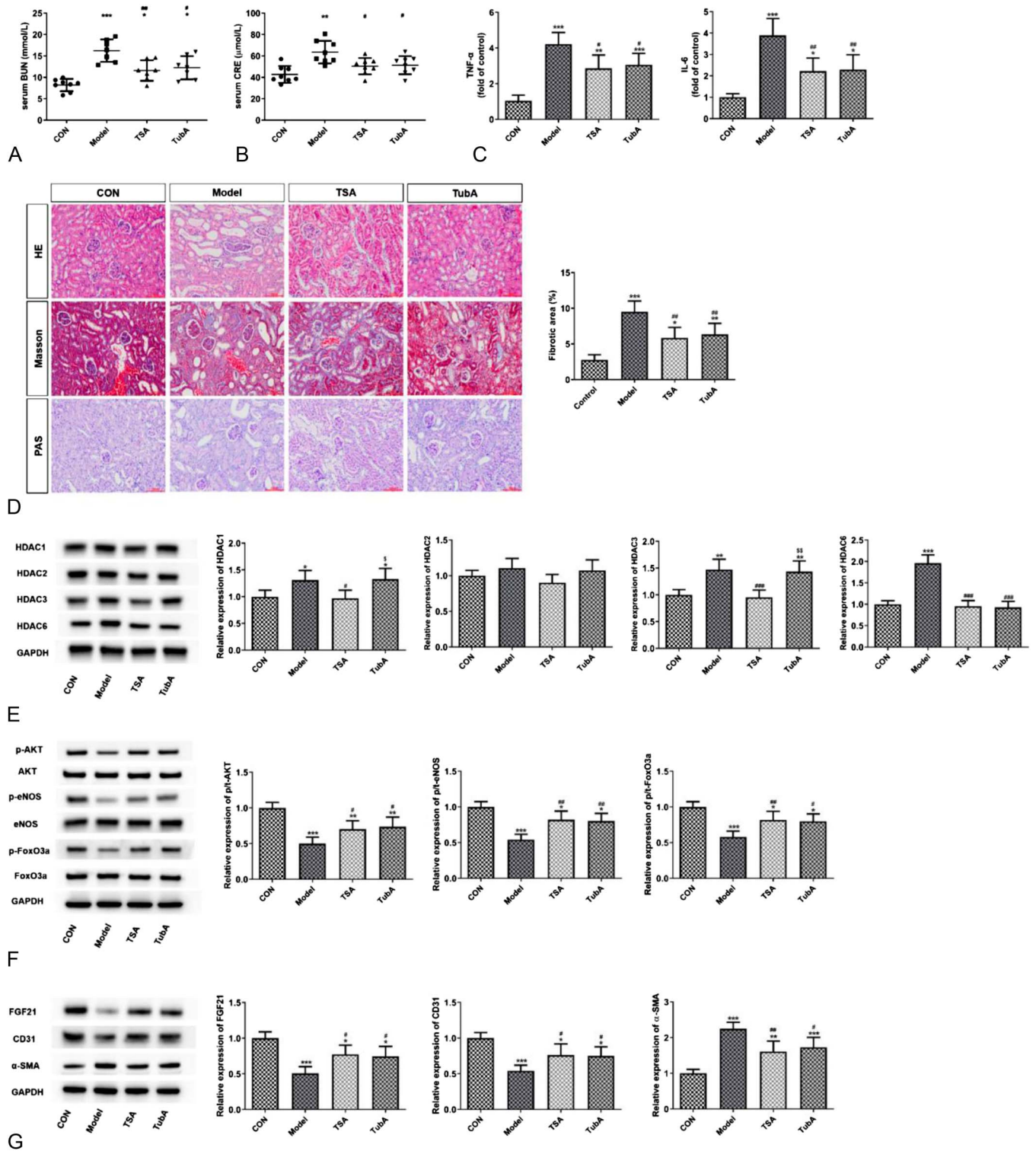


FIGURE 8. TSA or TubA alleviated renal inflammation and dysfunction in hyperuricemic mice. A, Serum BUN (n = 7–8). B, Serum CRE (n = 8). C, RT-qPCR analysis of TNF- α and IL-6 in renal tissues (n = 5). D, Representative images of mice renal tissue stained by H&E, Masson, and PAS (magnification $\times 200$), and percentage of fibrotic area was analyzed. E, WB analysis HDAC1, 2, 3, and 6 (n = 5). F, WB analysis of p-AKT/AKT, p-eNOS/eNOS, and p-FoxO3a/FoxO3a (n = 5). G, WB analysis of FGF21, CD31, and α -SMA (n = 5). One-way ANOVA followed by Tukey's post hoc multiple-group comparisons. * $P < 0.05$, ** $P < 0.001$, *** $P < 0.001$ versus CON; # $P < 0.05$, ## $P < 0.01$, ### $P < 0.001$ versus model; \$ $P < 0.05$, \$\$ $P < 0.01$ versus TSA.

subsequent experiments. The results showed that intracellular ROS generation in UA-stimulated HUVECs was significantly inhibited by TSA administration (Fig. 2A). In addition, TSA administration notably decreased UA-induced hypersecretion of inflammatory cytokines such as TNF- α , IL-1 β , and IL-6 (Fig. 2B). Besides, the nitric oxide (NO) level and the expression of endothelial nitric oxide synthase (eNOS) and AKT were detected. The results showed that NO level in HUVECs cotreated with TSA was higher than that in HUVECs stimulated with UA only (Fig. 2C). Moreover, the phosphorylated AKT and eNOS levels were upregulated by TSA treatment in a concentration-dependent fashion, while the total AKT and eNOS protein levels demonstrated no significant changes (Fig. 2G). In addition, the levels of myofibroblast marker α -SMA and endothelial cell marker CD31 were detected to explore the role of TSA in UA-stimulated endothelial-interstitial transformation. It was found that UA stimulation remarkably inhibited CD31 expression and enhanced α -SMA expression (Fig. 2D, E). By contrast, TSA treatment increased CD31 expression and decreased α -SMA expression (Fig. 2D–F), suggesting that TSA could inhibit UA-stimulated endothelial-interstitial transformation in HUVECs. As shown in Figure 2H–J, TSA administration significantly elevated FGF21 expression. ChIP assay demonstrated that the level of histone H3 acetylation on FGF21 promoter region was upregulated after TSA treatment. These data suggest that HDAC inhibitor may increase FGF21 expression in UA-stimulated HUVECs by enhancing the acetylated level of histone on FGF21 gene.

TSA Protects HUVECs Against High UA Exposure Through FGF21/PI3K/AKT Pathway

To examine whether FGF21 can mediate the effect of TSA on UA-induced VECI, the expression of FGF21 was downregulated by siRNA-FGF21 transfection. Owing to the more significant transfection efficiency, siRNA-FGF21-1 was selected in subsequent experiments (Fig. 3A). Interestingly, FGF21 downregulation abated the inhibitory effects of TSA on TNF- α , IL-1 β , and IL-6 expression levels (Fig. 3B) as well as ROS generation (Fig. 3C). More importantly, NO level and expression of p-eNOS and p-AKT in 12 mg/dL UA+TSA high+siRNA-FGF21 group were markedly lower than those in 12 mg/dL UA+TSA high group (Fig. 3D, E). Besides, FGF21 knockdown partially reversed the effect of TSA treatment on CD31 and α -SMA expression (Fig. 3F, G). These findings imply that FGF21 knockdown abrogates the protective effect of HDAC inhibitor against UA-induced VECI. TSA protected HUVECs against UA-induced VECI by upregulating FGF21 expression.

To further investigate the involvement of PI3K/AKT pathway, the PI3K inhibitor LY294002 was added into the ECM. After the addition of LY294002, the promotion of NO level and suppression of inflammatory cytokine mRNA expression levels by TSA were significantly reversed (Fig. 4A, B). In addition, LY294002 significantly inhibited phosphorylation of AKT, eNOS, and FoxO3a (Fig. 4C). As presented in Figure 4D, LY294002 significantly reversed the effects of TSA on protein expression of CD31 and α -SMA

but did not influence FGF21 expression in HUVECs. These data indicated that the activation of FGF21/PI3K/AKT pathways may mediate the protective effects of TSA on HUVECs.

TSA Increases FGF21 Expression in UA-stimulated HUVECs by Inhibiting HDAC6 Activity

To identify HDAC that mediates the protective effect of TSA, the activities of HDAC1, HDAC2, HDAC3, and HDAC6 in HUVECs were measured. Mocetinostat, an isoform-selective HDAC inhibitor, which specifically inhibits HDAC1, HDAC2, and HDAC3, was used to evaluate whether HDAC1-3 can mediate the protective effect of TSA. As shown in Figure 5A, the activities of HDACs, including HDAC1, HDAC2, HDAC3, and HDAC6, were remarkably higher in the UA group than in the CON group. TSA treatment markedly decreased the activities of HDAC1, HDAC2, HDAC3, and HDAC6, while Mocetinostat treatment did not influence HDAC6 activity. There was no difference in TNF- α , IL-1 β , and IL-6 expression and NO level between 12 mg/dL UA and 12 mg/dL UA+Mocetinostat groups (Fig. 5B, C). More importantly, compared with the 12 mg/dL UA group, Mocetinostat treatment did not increase the expression level of FGF21 (Fig. 5D, E). ChIP assay showed that there was no significant difference in histone H3 acetylation on FGF21 promoter region between 12 mg/dL UA and 12 mg/dL UA+Mocetinostat groups (Fig. 5F). Thus, it can be inferred that HDAC1, HDAC2, and HDAC3 do not mediate the protective effect of TSA.

HDAC6-siRNA was used to knock down HDAC6 mRNA in HUVECs to further confirm the role of HDAC6 in regulating the protective effects of HDAC inhibitors. SiRNA-HDAC6-1 was selected in subsequent experiments (Fig. 6A). After transfection with siRNA-HDAC6-1, HDAC6 activity decreased significantly (Fig. 6C). HDAC6 downregulation abated the effect of UA on the expression of inflammatory markers in HUVECs (Fig. 6B). At the same time, NO level and the expression levels of p-AKT, p-eNOS, and p-FoxO3a in 12 mg/dL UA+siRNA-HDAC6 group were higher than that in the 12 mg/dL UA group (Fig. 6D, F). Besides, HDAC6 knockdown partially reversed the effect of UA on CD31 and α -SMA expression (Fig. 6G). More importantly, compared with 12 mg/dL UA+NC group, the protein expression of FGF21 was significantly increased in the 12 mg/dL UA+siRNA-HDAC6 group (Fig. 6E). These data imply that HDAC6 downregulation has an effect similar to TSA treatment, and HDAC6 can mediate the protective effect of TSA.

TSA Treatment Attenuates Aorta and Kidney Injury in Hyperuricemia Mice

Consistent with the in vitro experiments, in vivo data indicated that HDACs, especially HDAC6 inhibitor, could attenuate UA-induced aortic and renal injury. As illustrated in Figure 7A, compared with the CON group, systolic blood pressure in the Model group slightly increased. There was no difference in diastolic blood pressure between groups. As presented in Figure 7B, C, serum UA in the Model,

TSA, and TubA groups was higher than that in the CON group, while serum NO was remarkably decreased in the Model group. After TSA or TubA administration for 4 consecutive weeks, the serum level of NO was significantly increased. There was no difference in serum FGF21 levels between the Model and CON groups, while TSA or TubA treatment significantly elevated serum FGF21 level (Fig. 7D). Moreover, TSA or TubA treatment notably decreased hyperuricemia-induced high levels of inflammatory cytokines in both serum and aorta tissue (Fig. 7E, F). The aorta from Model group had more severe damage in endothelium-dependent relaxation after Ach treatment compared with the CON group. This effect was reversed by TSA and TubA treatment. However, there was no difference in endothelium-independent relaxation between the study groups after SNP treatment (Fig. 7G). The histopathological analysis revealed that the structure of aorta was clear, with a tight arrangement of endothelial cells in the CON group, and there was no inflammatory cell aggregation in the vessel wall. Besides, edematous endothelial cells exhibited foam-like changes, while media thickness of thoracic aorta increased and structural disorder were observed in the Model group. However, compared with the Model group, the histopathological lesions were less severe in the TSA or TubA group. Smooth muscle cell proliferation was not obvious in the TSA or TubA group, and the cell structures were arranged in an orderly pattern (Fig. 7H). The results of Western blot showed that hyperuricemia upregulated the expression of HDAC1, HDAC3, and HDAC6 and had no obvious effect on HDAC2 expression in aorta tissues. TSA treatment reduced HDAC1,2,3,6 levels, while TubA could only reduce HDAC6 expression in aorta (Fig. 7I). AKT, eNOS, and FoxO3a phosphorylation levels in the Model group were all remarkably decreased compared with the CON group and significantly increased after TSA or TubA treatment (Fig. 7J). The levels of FGF21 and CD31 in the Model group were significantly decreased compared with those in the CON group. On the contrary, TSA or TubA administration dramatically increased the expression levels of CD31 and FGF21 (Fig. 7K).

It was found that both serum urea nitrogen (BUN) and creatinine (CRE) increased significantly in the Model group (Fig. 8A, B). TSA or TubA treatment dramatically reduced the levels of CRE and BUN, suggesting that TSA or TubA could effectively alleviate hyperuricemia-induced kidney injury. Similar to the effect on aorta, TSA or TubA treatment significantly reversed the high levels of inflammatory cytokines in renal tissue (Fig. 8C). Histological alterations of the kidney tissues were comprehensively examined by H&E, Masson's trichrome, and PAS staining (Fig. 8D). H&E and PAS staining of the kidney tissues in the Model group revealed obvious tubular damage and apoptosis, including tubular dilation and cell necrosis. Masson's staining showed that the fibrous tissue in the model group was increased compared with the CON group. The histopathological abnormalities of the kidneys were improved after TSA or TubA administration. As similar to the effect of hyperuricemia on aorta, HDAC1,3,6 protein levels in renal tissues were upregulated in the Model group. TSA downregulated HDAC1,3,6 protein

levels, while TubA only alleviated HDAC6 expression (Fig. 8E). In addition, TSA or TubA enhanced the phosphorylation levels of AKT, eNOS, and FoxO3a as well as promoted the expression of CD31 and FGF21 in kidney tissues (Fig. 8F, G). Altogether, these findings underscored hyperuricemia-induced inflammation and injury in aorta and kidney tissue and downregulated expression of FGF21. Consistent with the results of *in vitro* experiment, TSA or TubA treatment could significantly alleviate the injury of these organs and promote the expression of FGF21.

There were no obvious histopathological changes in the liver tissue of mice in each group, as examined by H&E staining (Supplementary Fig. 1A, <http://links.lww.com/JCVP/A883>). Different from aorta and kidney tissues, there was no difference in hepatic FGF21 expression between the CON and model groups, while TSA and TubA treatment significantly enhanced FGF21 expression in the liver (Supplementary Figure 1B, <http://links.lww.com/JCVP/A883>).

DISCUSSION

Our results, for the first time, demonstrated that HDAC inhibitor could alleviate UA-induced endothelial dysfunction both *in vitro* and *in vivo*. Hyperuricemia plays a pathogenic role in the occurrence of cardiovascular and renal diseases through endothelial inflammation and dysfunction.³⁸ Upregulation of HDACs has been reported to be a harbinger of uremic endothelial dysfunction.³⁹ However, the roles of HDACs in hyperuricemia remain unclear. Our results showed that TSA treatment significantly decreased UA-induced endothelial dysfunction, which uncovered a remarkable endothelial protective effect of HDAC inhibitors against hyperuricemia. However, the mechanisms behind the therapeutic benefit of HDAC inhibitors remain obscure. It is speculated that this protective effect of TSA may depend on the upregulated expression of FGF21 through inhibiting HDAC6 activity.

In this study, it was observed that UA stimulation led to the reduced expression of FGF21, and TSA recovered FGF21 expression in UA-stimulated HUVECs. FGF21 is an essential metabolic regulator which have been proved to protect vascular endothelial cells against oxidative stress-induced injury.⁴⁰ Emerging evidence revealed that FGF21 is a key factor in maintaining energy homeostasis and regulating systemic glucose and lipid metabolism.^{41,42} Overexpression of FGF21 in endothelial cells can reduce oxidative stress and improve endothelial function.⁴³ As for the role of FGF21 in UA-induced VECI, Rong and coworkers demonstrated that FGF21 could attenuate high UA-induced endothelial.⁴³ Our results demonstrated that FGF21 knockdown abrogated the suppressive effect of TSA on inflammatory factor release and ROS generation. Moreover, FGF21 knockdown aggravated UA-induced endothelial dysfunction and endothelial-interstitial transformation. Hence, TSA alleviated UA-induced VECI through upregulating FGF21 expression. Our study showed that the increased acetylation level of histone H3 on FGF21 promoter region after TSA treatment, which may reveal the

mechanism by which TSA enhances FGF21 expression in HUVECs.

Other studies have demonstrated that FGF21 could activate PI3K/AKT signaling in HUVECs.^{44,45} AKT is a serine/threonine protein kinase in mediator of PI3K/AKT signaling pathway, leading to the phosphorylation of multiple downstream molecules,⁴⁶ and plays critical and diverse roles in the cardiovascular system.^{46,47} PI3K/AKT pathways act as a positive regulator of endothelial NO synthase in endothelial cells. As a key enzyme, eNOS plays a crucial role in the generation of NO.⁴⁸ Phosphorylated PI3K/AKT can directly phosphorylate eNOS and then induce NO generation.⁴⁹ NO maintains vascular homeostasis through influences on vascular protection, including antioxidant, anti-inflammatory and antiproliferative effects.⁵⁰ Abnormal release of NO results in endothelial dysfunction.⁵¹ PI3K/AKT/eNOS axis has been shown to orchestrate protective effects on endothelial dysfunction.^{49,52} FoxO3a, one of the FoxO family members, is another important downstream target of the PI3K/AKT pathway. Activated AKT phosphorylates FoxO3a leading to the registered shift of FoxO3a from nucleus to cytoplasm, which could inhibit ROS and apoptosis.⁵³ Guo reported FGF21 could inhibit HUVEC apoptosis through activating PI3K/AKT/FoxO3a pathway manifested by the increased phosphorylation levels of AKT and FoxO3a.⁴⁵ In our study, UA stimulation inhibited the production of NO and TSA treatment elevated NO level and expressions of p-AKT, p-eNOS, and p-FoxO3a both *in vitro* and *in vivo*. In addition, we also proved TSA abated UA-induced inflammation, oxidative stress, and endothelial–interstitial transformation in HUVECs. However, these protective effects disappeared after the use of PI3K/AKT pathway inhibitor LY294002. Thus, HDAC inhibitors ameliorated UA-induced endothelial cell injury by inhibiting inflammation, oxidative stress, and endothelial–interstitial transformation by activating PI3K/AKT axis.

As a nonselective HDAC inhibitor, TSA has been proved to exert multiple cardioprotective effects. In this study, we found that TSA alleviated UA-induced VECI. However, it is necessary to determine the relationship of HDAC isoform and disease pathogenesis and to develop HDAC inhibitor with high selectivity and specificity to decrease undesirable off-target effects. Our results also showed that UA stimulation induced the upregulation of HDAC6 in a concentration-dependent manner. Wang *et al*⁵⁴ showed that the inhibition of HDAC6 catalytic activity could upregulate FGF21 expression in the central nervous system. To further demonstrate whether HDAC6 inhibitor could mediate the protection of vascular endothelial cells, Mocetinostat, a selective HDAC1-3 inhibitor, was selected to exclude the effects of other HDACs. The results demonstrated that Mocetinostat effectively inhibited HDAC1-3 activities but had no influence on HDAC6 activity. Besides, Mocetinostat did not significantly elevate NO level and reduce inflammatory response in HUVECs. More importantly, Mocetinostat did not enhance FGF21 expression in HUVECs. Although it is a HDAC inhibitor, Mocetinostat did not elevate the acetylated level of FGF21 promoter region. These results showed that HDAC1-3 did not mediate

the protective effect of TSA. Besides, HDAC6 knockdown significantly alleviated UA-induced endothelial dysfunction and recovered FGF21 expression in UA-stimulated HUVECs. Hence, TSA may alleviate UA-induced VECI by inhibiting HDAC6 activity.

Our *in vivo* study showed hyperuricemia could lead to VECI manifested in both aortic and renal damage, including increased inflammatory factors and decreased vascular endothelial function and endothelial–interstitial transformation. Both TSA and selective HDAC6 inhibitor TubA showed anti-inflammatory effects, organ protection, and inhibition of endothelial–interstitial transformation in aortic and renal tissues. Although hyperuricemia affected HDAC6 expression and slightly increased the expression of HDAC1 and HDAC3, TubA showed the same protective effect as TSA, which further indicated that HDAC6 mediated VECI induced by hyperuricemia. Consistent with the results of *in vitro* experiments, both TSA and TubA significantly increased FGF21 expression and promoted AKT, eNOS, and FoxO3a phosphorylation levels in aorta and kidney tissues. These results suggest that TSA alleviates VECI in mice through HDAC6/FGF21/PI3K/AKT pathways. Some studies showed that HDAC3 inhibitor could stimulate FGF21 expression in mouse liver tissue,⁵⁵ while others demonstrated that HDAC6 inhibition could stimulate the expression of FGF21.⁵⁴ Our *in vitro* and *in vivo* experiments showed that HDAC6 inhibitor enhanced FGF21 expression and ameliorated UA-induced VECI.

Slightly different from the *in vitro* results, the effect of TSA on FGF21 expression *in vivo* may be more complex. FGF21 belongs to the endocrine subfamily of FGFs that is mainly expressed and secreted in the liver.⁵⁶ FGF21 can bind with fibroblast growth factor receptors on vascular endothelial cells to exert physiological functions.⁵⁷ There are few studies about how UA influence FGF21 expression in liver tissues. Chen *et al*⁵⁸ demonstrated that UA stimulation suppressed FGF21 expression by upregulating miR-149-5p expression in hepatocytes. Previous research showed that HDAC inhibitors increased serum FGF21 level by promoting the secretion of FGF21 in mouse liver tissue.⁵⁵ Our study indicated that hyperuricemia did not significantly alter FGF21 in serum and liver tissue but significantly reduced FGF21 expression in aorta and renal tissues, while TSA or TubA treatment could significantly increase the level of FGF21 in serum, aorta, renal, and liver tissues in hyperuricemia mice. Thus, we hypothesize that the increased serum FGF21 may be attributed to the fact that TSA or TubA treatment can improve FGF21 expression and secrete it to the circulatory system. The increased serum FGF21 acts on vascular endothelial cells and reduces hyperuricemia-induced VECI.

CONCLUSION

To the best of our knowledge, this study is the first to demonstrate that HDAC inhibitors ameliorate UA-induced VECI by inhibiting HDAC6 and regulating FGF21 expression. HDACs, especially HDAC6, can serve as a novel target for treating hyperuricemia-induced endothelial dysfunction.

REFERENCES

- Wang Q, Wen X, Kong J. Recent progress on uric acid detection: a review. *Crit Rev Anal Chem*. 2020;50:359–375.
- Kanbay M, Segal M, Afsar B, et al. The role of uric acid in the pathogenesis of human cardiovascular disease. *Heart*. 2013;99:759–766.
- Jung SW, Kim S-M, Kim YG, et al. Uric acid and inflammation in kidney disease. *Am J Physiol-Renal Physiol*. 2020;318:F1327–F1340.
- Schwartz IF, Grupper A, Chernichovski T, et al. Hyperuricemia attenuates aortic nitric oxide generation, through inhibition of arginine transport, in rats. *J Vasc Res*. 2011;48:252–260.
- Kang D-H, Park S-K, Lee I-K, et al. Uric acid-induced C-reactive protein expression: implication on cell proliferation and nitric oxide production of human vascular cells. *J Am Soc Nephrol*. 2005;16:3553–3562.
- Singh C, Jain S, Dhawan V, et al. Uric acid as a predictor of endothelial dysfunction in patients with metabolic syndrome. *Arch Endocrinol Metab*. 2021;64:810–815.
- Zhu GH, Sun XP, Li J, et al. Association between serum uric acid level and endothelial dysfunction in elderly individuals with untreated mild hypertension. *J Geriatr Cardiol*. 2020;17:264–269.
- Marchio P, Guerra-Ojeda S, Vila JM, et al. Targeting early atherosclerosis: a focus on oxidative stress and inflammation. *Oxidative Med Cell Longevity*. 2019;2019:1–32.
- Seto E, Yoshida M. Erasers of histone acetylation: the histone deacetylase enzymes. *Cold Spring Harbor Perspect Biol*. 2014;6:a018713.
- Li P, Ge J, Li H. Lysine acetyltransferases and lysine deacetylases as targets for cardiovascular disease. *Nat Rev Cardiol*. 2020;17:96–115.
- Chun P. Therapeutic effects of histone deacetylase inhibitors on heart disease. *Arch Pharm Res*. 2020;43:1276–1296.
- Schuetz KB, McKinsey TA, Long CS. Targeting cardiac fibroblasts to treat fibrosis of the heart: focus on HDACs. *J Mol Cell Cardiol*. 2014;70:100–107.
- Yang J, He J, Ismail M, et al. HDAC inhibition induces autophagy and mitochondrial biogenesis to maintain mitochondrial homeostasis during cardiac ischemia/reperfusion injury. *J Mol Cell Cardiol*. 2019;130:36–48.
- Kee HJ, Eom GH, Joung H, et al. Activation of histone deacetylase 2 by inducible heat shock protein 70 in cardiac hypertrophy. *Circ Res*. 2008;103:1259–1269.
- Wang K, Tang R, Wang S, et al. SAHA could inhibit TGF- β 1/p38 pathway in MI-induced cardiac fibrosis through DUSP4 overexpression. *Heart Vessels*. 2022;37:152–160.
- Herr DJ, Baarine M, Aune SE, et al. HDAC1 localizes to the mitochondria of cardiac myocytes and contributes to early cardiac reperfusion injury. *J Mol Cell Cardiol*. 2018;114:309–319.
- Lugenbiel P, Govorov K, Syren P, et al. Epigenetic regulation of cardiac electrophysiology in atrial fibrillation: HDAC2 determines action potential duration and suppresses NRSF in cardiomyocytes. *Basic Res Cardiol*. 2021;116:13.
- Na J, Jin H, Wang X, et al. The crosstalk of HDAC3, microRNA-18a and ADRB3 in the progression of heart failure. *Cell Biosci*. 2021;11:31.
- Samant SA, Courson DS, Sundaesan NR, et al. HDAC3-dependent reversible lysine acetylation of cardiac myosin heavy chain isoforms modulates their enzymatic and motor activity. *J Biol Chem*. 2011;286:5567–5577.
- Lee H-A, Lee D-Y, Cho H-M, et al. Histone deacetylase inhibition attenuates transcriptional activity of mineralocorticoid receptor through its acetylation and prevents development of hypertension. *Circ Res*. 2013;112:1004–1012.
- Saito S, Lasky JA, Guo W, et al. Pharmacological inhibition of HDAC6 attenuates endothelial barrier dysfunction induced by thrombin. *Biochem Biophysical Res Commun*. 2011;408:630–634.
- Leucker TM, Nomura Y, Kim JH, et al. Cystathionine γ -lyase protects vascular endothelium: a role for inhibition of histone deacetylase 6. *Am J Physiol-Heart Circulatory Physiol*. 2017;312:H711–H720.
- Chen J, Zhang J, Shaik NF, et al. The histone deacetylase inhibitor tubacin mitigates endothelial dysfunction by up-regulating the expression of endothelial nitric oxide synthase. *J Biol Chem*. 2019;294:19565–19576.
- Yu J, Ma M, Ma Z, et al. HDAC6 inhibition prevents TNF- α -induced caspase 3 activation in lung endothelial cell and maintains cell-cell junctions. *Oncotarget*. 2016;7:54714–54722.
- Batchu SN, Brijmohan AS, Advani A. The therapeutic hope for HDAC6 inhibitors in malignancy and chronic disease. *Clin Sci*. 2016;130:987–1003.
- Ke B, Chen Y, Tu W, et al. Inhibition of HDAC6 activity in kidney diseases: a new perspective. *Mol Med*. 2018;24:33.
- Yan S, Wei X, Jian W, et al. Pharmacological inhibition of HDAC6 attenuates NLRP3 inflammatory response and protects dopaminergic neurons in experimental models of Parkinson's disease. *Front Aging Neurosci*. 2020;12:78.
- Chen X, Yu C, Hou X, et al. Histone deacetylase 6 inhibition mitigates renal fibrosis by suppressing TGF- β and EGFR signaling pathways in obstructive nephropathy. *Am J Physiol-Renal Physiol*. 2020;319:F1003–F1014.
- Shi Y, Xu L, Tang J, et al. Inhibition of HDAC6 protects against rhabdomyolysis-induced acute kidney injury. *Am J Physiol-Renal Physiol*. 2017;312:F502–F515.
- Karagiannis TC, Lin AJE, Ververis K, et al. Trichostatin A accentuates doxorubicin-induced hypertrophy in cardiac myocytes. *Aging (Albany NY)*. 2010;2:659–668.
- Liu F, Levin MD, Petrenko NB, et al. Histone-deacetylase inhibition reverses atrial arrhythmia inducibility and fibrosis in cardiac hypertrophy independent of angiotensin. *J Mol Cell Cardiol*. 2008;45:715–723.
- Hebbel RP, Vercellotti GM, Pace BS, et al. The HDAC inhibitors trichostatin A and suberoylanilide hydroxamic acid exhibit multiple modalities of benefit for the vascular pathobiology of sickle transgenic mice. *Blood*. 2010;115:2483–2490.
- Hakami NY, Dusing GJ, Peshavariya HM. Trichostatin A, a histone deacetylase inhibitor suppresses NADPH oxidase 4-derived redox signalling and angiogenesis. *J Cell Mol Med*. 2016;20:1932–1944.
- Zhou L, Wei B, Wu L, et al. Anti-hyperuricemia activity and toxicity prediction of a novel xanthine oxidoreductase inhibitor. *Biomed Chromatogr BMC*. 2020;34:e4727.
- Ooi JYY, Tuano NK, Rafehi H, et al. HDAC inhibition attenuates cardiac hypertrophy by acetylation and deacetylation of target genes. *Epigenetics*. 2015;10:418–430.
- Shen Z, Ji K, Cai Z, et al. Inhibition of HDAC6 by Tubastatin A reduces chondrocyte oxidative stress in chondrocytes and ameliorates mouse osteoarthritis by activating autophagy. *Aging (Albany NY)*. 2021;13:9820–9837.
- Wilde E, Aubdool AA, Thakore P, et al. Tail-cuff technique and its influence on central blood pressure in the mouse. *J Am Heart Assoc*. 2017;6:e005204.
- Mallat SG, Al Kattar S, Tanius BY, et al. Hyperuricemia, hypertension, and chronic kidney disease: an emerging association. *Curr Hypertens Rep*. 2016;18:74.
- Palomo M, Vera M, Martin S, et al. Up-regulation of HDACs, a harbinger of uraemic endothelial dysfunction, is prevented by defibrotide. *J Cell Mol Med*. 2020;24:1713–1723.
- Zhu W, Wang C, Liu L, et al. Effects of fibroblast growth factor 21 on cell damage in vitro and atherosclerosis in vivo. *Can J Physiol Pharmacol*. 2014;92:927–935.
- Alonge KM, Meares GP, Hillgartner FB. Glucagon and insulin cooperatively stimulate fibroblast growth factor 21 gene transcription by increasing the expression of activating transcription factor 4. *J Biol Chem*. 2017;292:5239–5252.
- Brahma MK, Adam RC, Pollak NM, et al. Fibroblast growth factor 21 is induced upon cardiac stress and alters cardiac lipid homeostasis. *J Lipid Res*. 2014;55:2229–2241.
- Ouyang R, Zhao X, Zhang R, et al. FGF21 attenuates high uric acid-induced endoplasmic reticulum stress, inflammation and vascular endothelial cell dysfunction by activating Sirt1. *Mol Med Rep*. 2021;25:35.
- Li Y, Huang J, Jiang Z, et al. FGF21 inhibitor suppresses the proliferation and migration of human umbilical vein endothelial cells through the eNOS/PI3K/AKT pathway. *Am J Transl Res*. 2017;9:5299–5307.
- Guo D, Xiao L, Hu H, et al. FGF21 protects human umbilical vein endothelial cells against high glucose-induced apoptosis via PI3K/Akt/Fox3a signaling pathway. *J Diabetes its Complications*. 2018;32:729–736.
- Abeyrathna P, Su Y. The critical role of Akt in cardiovascular function. *Vasc Pharmacol*. 2015;74:38–48.
- Chaanine AH, Hajjar RJ. AKT signalling in the failing heart. *Eur J Heart Fail*. 2011;13:825–829.
- Kolluru GK, Siamwala JH, Chatterjee S. eNOS phosphorylation in health and disease. *Biochimie*. 2010;92:1186–1198.
- Lin F, Yang Y, Wei S, et al. Hydrogen sulfide protects against high glucose-induced human umbilical vein endothelial cell injury through

- activating PI3K/Akt/eNOS Pathway<. *Drug Des Dev Ther.* 2020;14:621–633.
50. Siragusa M, Fleming I. The eNOS signalosome and its link to endothelial dysfunction. *Pflügers Archiv - Eur J Physiol.* 2016;468:1125–1137.
 51. Taneja G, Sud A, Pendse N, et al. Nano-medicine and vascular endothelial dysfunction: options and delivery strategies. *Cardiovasc Toxicol.* 2019;19:1–12.
 52. Hu L, Sun Y, Hu J. Catalpol inhibits apoptosis in hydrogen peroxide-induced endothelium by activating the PI3K/Akt signaling pathway and modulating expression of Bcl-2 and Bax. *Eur J Pharmacol.* 2010;628:155–163.
 53. Wu Z, Huang A, Yan J, et al. Resveratrol ameliorates cardiac dysfunction by inhibiting apoptosis via the PI3K/Akt/FoxO3a pathway in a rat model of diabetic cardiomyopathy. *J Cardiovasc Pharmacol.* 2017;70:184–193.
 54. Wang Z, Leng Y, Wang J, et al. Tubastatin A, an HDAC6 inhibitor, alleviates stroke-induced brain infarction and functional deficits: potential roles of α -tubulin acetylation and FGF-21 upregulation. *Sci Rep.* 2016;6:19626.
 55. Zhang J, Xu Z, Gu J, et al. HDAC3 inhibition in diabetic mice may activate Nrf2 preventing diabetes-induced liver damage and FGF21 synthesis and secretion leading to aortic protection. *Am J Physiol-Endocrinology Metab.* 2018;315:2E150–E162.
 56. Tabari FS, Karimian A, Parsian H, et al. The roles of FGF21 in atherosclerosis pathogenesis. *Rev Endocr Metab Disord.* 2019;20:103–114.
 57. Beenken A, Mohammadi M. The structural biology of the FGF19 subfamily. *Adv Exp Med Biol.* 2012;728:1–24.
 58. Chen S, Chen D, Yang H, et al. Uric acid induced hepatocytes lipid accumulation through regulation of miR-149-5p/FGF21 axis. *BMC Gastroenterol.* 2020;20:39.